PCCP

Accepted Manuscript

ROYAL SOCIETY OF CHEMISTRY

www.rsc.org/pccp

Journal Name

COMMUNICATION

Re-examining the Chevrel phase Mo_6S_8 cathode for Mg intercalation from an electronic structure perspective

Received 00th January 20xx,
Accepted 00th January 20xx

DOI: 10.1039/x0xx00000x

www.rsc.org/

Florian Thöle,[a] Liwen F. Wan[b] and David Prendergast*[b†]

We re-examine the electronic response of the Chevrel phase Mo_6S_8 upon Mg intercalation. The ground-state Mo_6S_8 is metallic and exhibits strongly localized electronic screening of Mg^{2+} ions. This localized screening cloud effectively shields the 2+ charge carried by Mg ions on the length scale of one unit cell that facilitates Mg ion diffusion.

Compared to monovalent Li-ion batteries, divalent Mg-ion technologies offer one means of increasing theoretical capacity and energy density, merely by doubling the number of electrons stored per ion. The first working Mg battery prototype was established in 2000, [1] but suffers from a low operating voltage (~ 1.1 V). The theoretical cell voltage is determined by the chemical potential difference between the anode and cathode. [2] In the case of Mg batteries, the optimal anode material is Mg metal, which exhibits a low electrode potential while providing a rich source of Mg ions. The search for cathode materials, however, is more challenging because ion intercalation processes involve two concerted steps: ion diffusion and local electron transport to maintain charge neutrality. [3,4] In this sense, the practical use of most high-voltage cathode materials is limited by poor ionic diffusivity, due to the formation of strong chemical bonds with Mg.

In fact, the realization of the first working Mg battery relies on the use of the low-voltage Chevrel phase (CP) Mo_6S_8, as the cathode material. [1,5,6] It is proposed that the relatively high mobility of Mg ions in these CP structures is attributable to the fast redistribution of electronic charge over the Mo_6 cluster, where it acts as a rigid unit to change oxidation state. [3,4] This argument has successfully taken into account the effects of forming a metal cluster with non-directional metallic bonding. However, it assumes the chemical potential is still determined by the redox couple of Mo, analogous to other transition metal oxides such as CoO_2, $FePO_4$ and MnO_2. [7] In these transition metal compounds, the Fermi level is set primarily by the redox couple of the transition metal because the binding energies of valence electrons in the O^{2-} p-states reside well below those of the transition metal d-states. [7] When the anion p-states arise to the top of valence band and become dominant, the redox reaction may occur at the anions instead of the transition metals. [8,9]

Furthermore, unlike conventional transition metal oxides that are most semiconductors or insulators, the CP structures exhibits metallic ground states and can therefore provide fast electronic screening of intercalating ions. [10] In this work, we revisit the electronic structure of $Mg_xMo_6S_8$ in its de-magnesiated (x=0), half-magnesiated (x=1) and fully-magnesiated (x=2) states, and examine the origin of high Mg ion mobility as it relates to a proposed localized electronic screening.

Here the electronic structure of CP is studied using density functional theory (DFT) with a plane-wave representation of the electronic wavefunctions. [11,12] Ultrasoft pseudopotentials, found in the Quantum Espresso pseudopotential library, [12,13] are used to describe electron-ion interactions. The Perdew-Burke-Ernzerhof (PBE) generalized-gradient approximation (GGA) is used to capture the exchange-correlation potential. [14] To ensure the convergence of our unit-cell calculations, the plane-wave basis is truncated at 50 Ry and a uniform k-point grid of 5×5×5 is used to integrate the first Brillouin zone in reciprocal space. [15]

In addition, an on-site Coulomb interactions parameter (the so-called Hubbard U term) is added to provide stronger Coulomb repulsion for Mo 4d electrons. The U parameter is calculated for bulk Mo_6S_8 from first-principles using the self-consistent linear response approach. [16,17] The obtained U value of 3.16 eV is subsequently used in all of our simulations to study the electronic response of Mo_6S_8 upon magnesiation. As a comparison, the results using standard GGA functional are provided in the supplementary material.

Using the GGA+U approach, we predict the ground-state structures of Mo_6S_8, $MgMo_6S_8$ and $Mg_2Mo_6S_8$ as shown in table 1. Upon half-magnesiation, Mg occupies one of the lower energy inner sites, which are arranged hexagonally around the rhombohedral axis. [18] Due to the periodic boundary conditions in our DFT simulations, the

[a] Materials Theory, Department of Materials, ETH Zürich, Zürich, Switzerland 8093
[b] Joint Center for Energy Storage Research (JCESR), The Molecular Foundry, Lawrence Berkeley National Laboratory, Berkeley, California, United State 94720
† E-mail: dgprendergast@lbl.gov

Table 1: Calculated lattice parameters of Mo_6S_8, $MgMo_6S_8$, and $Mg_2Mo_6S_8$ at U = 3.16 eV. The experimental values are taken from Ref. [18]

Structure	Methods	a (Å)	b (Å)	c (Å)	α (°)	β (°)	γ (°)
Mo_6S_8	GGA+U	6.446	-	-	91.50	-	-
	Exp.	6.429	-	-	91.27	-	-
$MgMo_6S_8$	GGA+U	6.508	6.514	6.509	92.79	92.79	93.67
	Exp.	6.494	-	-	93.43	-	-
$Mg_2Mo_6S_8$	GGA+U	6.562	-	-	92.82	-	-
	Exp.	6.612	-	-	95.17	-	-

same inner site is repeatedly taken in all unit cells and, as a result, breaks the rhombohedral symmetry of the entire lattice. In reality, according to diffraction, the inner sites are occupied either randomly or with some long-range order that preserves the rhombohedral symmetry. [18] Upon fully magnesiation, Mg simultaneously occupy one of the inner sites (0.108, -0.029, -0.091) and one of the outer sites (-0.074, 0.017, 0.385). With the R-3 symmetry constraint, we relax the unit cell of $Mg_2Mo_6S_8$ and summarize the results in table 1.

Based on the structures presented in table 1, we present GGA+U Kohn-Sham electronic density of states for Mo_6S_8, $MgMo_6S_8$, and $Mg_2Mo_6S_8$ in figure 1. In the de-magnesiated state, Mo_6S_8 is metallic, and the electronic states at the Fermi level comprise a mixture of Mo 4d and S 3p states. About 1 eV above the Fermi energy, there is a dip in the density of states called the "pseudo" gap. [19] For half-magnesiated $MgMo_6S_8$, the pseudo gap is widened with the Fermi level close by. In addition, some slight changes of Mo 4d and S 3p states are observed, which are likely due to the charge redistribution upon Mg insertion (see below). When the cell is fully magnesiated, the valence bands are completely filled by the four neutralizing electrons per unit cell and the band gap is opened to realize a metal-to-semiconductor transition. We note that because of expected limitations in our chosen DFT exchange correlation functional, we likely underestimate the band gap size. For example, the gap is not entirely opened in $Mg_2Mo_6S_8$ when using the standard PBE-GGA functional as shown in the supplementary material. With the U correction, the gap in $Mg_2Mo_6S_8$ is estimated as ~ 0.5 eV whereas using more sophisticated HSE hybrid functional, the gap is predicted as ~ 2 eV. Despite this well-known band gap error, the observed metal-to-semiconductor transition upon magnesiation is still valid and, so, we retain the same GGA+U approach that enables us to scale our simulations to much larger length scales.

To provide more insight regarding the local change in electronic structure in the vicinity of intercalated Mg ion, we calculate the charge density difference (charge rearrangement) of a 3×3×3 Mo_6S_8 supercell before and after Mg insertion, *i.e.* $\Delta\rho = \rho_{Mg(Mo6S8)27} - \rho_{(Mo6S8)27}$. The supercell is fully relaxed with one Mg at the inner site. The obtained charge density difference is rendered in figure 2 at an isosurface level of 0.002 e/Å^3. The strongest charge localization is observed around Mg and the charge density on the transition metal ions varies very little. To obtain a quantitative measurement of the changes in charge density, we compute the Bader charge difference between $Mg(Mo_6S_8)_{27}$ and $(Mo_6S_8)_{27}$. In the inset of figure 2, the Bader charge differences of all Mo and S atoms are represented with respect to their distance to the inserted Mg. A positive Δe value indicates the atom is gaining electrons, whereas negative means the atom is losing electrons. During magnesiation, electronic

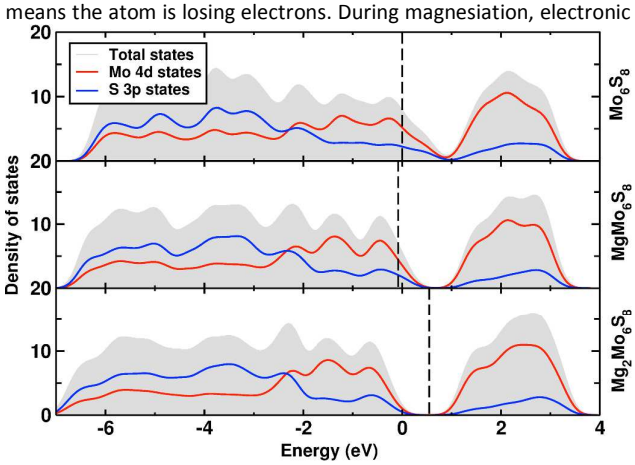

Figure 1: Electronic density of states for Mo_6S_8, $MgMo_6S_8$ and $Mg_2Mo_6S_8$. The total densities of states are presented by the shaded area and the projected Mo 4d and S 3p states are shown in red and blue curves. The dashed vertical lines represent the position of the Fermi energy for different structures. The Fermi energy of Mo_6S_8 is arbitrarily set as energy zero and the states are all aligned with respected to Mo 4p states far below energy zero.

screening is evident as a change in electron density on those S atoms within a distance of 4 Å of the intercalated Mg ion.

Since there is no significant electron density increase on the Mo_6 clusters, *i.e.* Mo does not charge its formal oxidation state, we expect a small volume change of Mo_6 upon Mg intercalation. In table 2, the Mo-Mo distance within the Mo_6 cluster is tabulated and compared for various Mg intercalated structures. d_1 and d_2 denote two inequivalent distances in the cluster with rhombohedral symmetry. For ground-state Mo_6S_8, our GGA+U predicted d_1 and d_2 values match very well with experiment. [18] When the rhombohedral symmetry is broken, as for the case of $MgMo_6S_8$ and $Mg_2Mo_6S_8$, the range of d_1 and d_2 values evident in our finite supercell models are indicated. Again, our results are in excellent agreement with experiment for Mg intercalated CP structures, although in experiment the overall symmetry is preserved on average. [18]

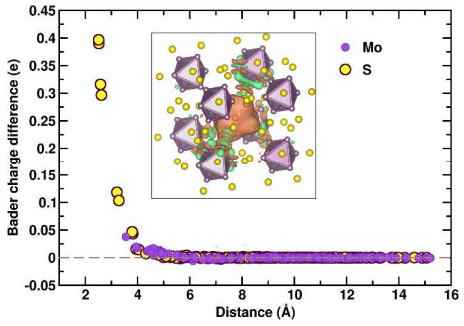

Figure 2: Bader charge differences for Mo and S upon Mg insertion. Inset shows the charge density difference between a system with Mg at an inner position and the system without Mg. Mo, S and Mg are shown in purple, yellow and orange, respectively. Red surfaces signify gain of charge, and green surfaces signify loss of charge. To

facilitate the visualization, only the Mo_6S_8 units next to Mg are shown in the figure.

Table 2: Mo-Mo distances in the Mo_6 cluster for different charge state of $MgMo_6S_8$. The results are compared with the calculated distances in $Mg_xMo_6S_8$ as well as experiment. [18]

Geometry factors	No additional e^- (Mo_6S_8)		
	DFT	Exp.	
d_1	2.70 Å	2.67 Å	
d_2	2.85 Å	2.86 Å	
	2 additional e^-		
	$[Mo_6S_8]^{2-}$	$MgMo_6S_8$	
	DFT	DFT	Exp.
d_1	2.60 Å	2.66-2.68 Å	2.68 Å
d_2	2.60 Å	2.74-2.76 Å	2.74 Å
	4 additional e^-		
	$[Mo_6S_8]^{4-}$	$Mg_2Mo_6S_8$	
	DFT	DFT	Exp.
d_1	2.58 Å	2.64-2.66 Å	2.66 Å
d_2	2.58 Å	2.71 Å	2.67

To further test the ability of Mo_6 to accept electrons, in the absence of Mg ions (but in the presence of a neutralizing uniform background charge density), we add 2 or 4 electrons (per unit cell) to Mo_6S_8 and calculate the resulting relaxed Mo-Mo bond length. As shown in table 2, d_1 and d_2 values for electron enriched Mo_6S_8 unit cells exhibit large deviations from their Mg intercalated counterparts because additional electrons fill up Mo 4d states. This comparison confirms that, upon intercalation, neutralizing electrons do not reside entirely (nor predominantly) on the Mo_6 clusters and, so, the cluster do not change their formal oxidation state. If extra electrons were accumulated on Mo_6 clusters, a significant reduction in Mo-Mo bond lengths within the Mo_6 clusters would be evident, which is not the case for $MgMo_6S_8$ nor $Mg_2Mo_6S_8$. The observed overall lattice change in table 1 is mainly attributed to the dilation of the S cage, because some of the S atoms next to Mg are electron enriched. Note that a similar but smaller local enrichment was observed for S atoms in TiS_2 upon lithiation. [8]

The results of our electronic structure analysis lead us to re-examine previous arguments about why the CP cathode performs well for Mg intercalation. Previously, it was assumed that the Mo_6 cluster is reduced upon Mg insertion. However, our results show that the delocalized Mo 4d states are not occupied during Mg intercalation, and, as such, the Mo_6 unit does not act as a classical redox center. The neutralizing electrons redistribute proximally around the Mg ion to form a screening cloud that can effectively shield its 2+ charge, reducing ion-ion repulsion between intercalants. The concept of shielding the multivalent charge of Mg^{2+} is not new. For example, to improve the poor ion mobility of Mg in V_2O_5 (due to strong ionic bonds with under-coordinated O atoms along the diffusion pathways) one strategy is to provide an aqueous solvation sphere (shielding the ion from strong bonding interactions) [4]. The advantage of CP in this regard is that the screening takes place natively in the host due to its unique metallic electronic structure.

The fact that Mo does not serve as a redox center is because of the presence of Mo_6 clusters. Within Mo_6, electronic bonding is non-directional and orbitals are highly delocalized. According to the electron-counting rule to form octahedral clusters, 24 electrons are needed from Mo_6 to saturate 12 uniform bonds in the cluster. [20] Consequently, the entire cluster becomes charged as Mo_6^{12+} and donates the extra 12 electrons to the S cage. However, to reach the inert gas electron configuration of S, 16 electrons need to be transferred. As a result, the intrinsic Mo_6S_8 unit is deficient by 4 electrons. When two Mg ions are intercalated into the open sites between Mo_6S_8 units, 4 additional neutralizing electrons (per unit cell) arrive and stabilize the electron deficient Mo_6S_8 structure. Therefore, strictly speaking there is no traditional transition-metal redox reaction occurring during Mg intercalation. The intercalation of Mg ions satisfies the electronic configuration of S atoms instead and shifts the Fermi level of Mo_6S_8 into its pseudo gap, *i.e.*, inducing a metal to semiconductor transition. This mechanism also implies that adding more than 4 electrons will likely start filling up the Mo 4d anti-bonding states and thus decrease the electronic stability of the host compound.

In summary, we have analyzed the electronic response of the Chevrel phase Mo_6S_8 upon the intercalation of divalent Mg ions. The metallic electronic structure of Mo_6S_8 allows for highly localized electronic screening that shields the charge of Mg^{2+}. As a result, Mg ions can diffuse more easily in the lattice. Our calculated Mg^{2+} diffusion barrier is ~0.5 eV at 0K in the dilute limit (one Mg in a 2×2×2 Mo_6S_8 supercell), which can be converted to an ion diffusion constant of ~10^{-12} cm^2/s. Compared to other traditional semiconducting or insulating hosts (*e.g.*, oxides, phosphates, etc.), better mobility of Mg ions is achieved in the Chevrel phase structure [4,21] due to its intrinsic metallic response, although for the same reason, the cathode voltage may be diminished.

The search for intercalating cathode materials can be expanded beyond transition metal compounds, which rely primarily on changes in transition metal oxidation state to maintain local charge neutrality. Intrinsically electron-deficient cluster materials [22] also show the capability of accepting electrons and therefore may serve as effective host materials for intercalation of multivalent ions.

This work was supported by the Joint Center for Energy Storage Research, an Energy Innovation Hub funded by the U.S. Department of Energy, Office of Science, Basic Energy Sciences. The computations were performed through a User Project at The Molecular Foundry using the local cluster (vulcan), which is managed by the High Performance Computing Services Group, at Lawrence Berkeley National Laboratory.

Notes and references

1 D. Aurbach, Z. Lu, A. Schechter, Y. Gofer, H. Gizbar, R. Turgeman, Y. Cohen, M. Moshkovich and E. Levi, *Nature*, 2000, **407**, 724.
2 G. Ceder, M.K. Aydinol and A.F. Kohan, *Comput. Mat. Sci.,* 1997, **8**, 161.
3 E. Levi, M.D. Levi, O. Chasid and D. Aurbach, *J. Electroceram.*, 2009, **22**, 13.
4 E. Levi, Y. Gofer and D. Aurbach, *Chem. Mater.*, 2010, **22**, 860.
5 M.D. Levi, E. Lancri, E. Levi, H. Gizbar, Y. Gofer and D. Aurbach, *Solid State Ionics*, 2005, **176**, 1695.
6 M.D. Levi, E. Lancry, H. Gizbar, Z. Lu, E. Levi, Y. Gofer and D. Aurbach, *J. Electrochem. Soc.,* 2004, **151**, A1044.

7 J.B. Goodenough and Y. Kim, *Chem. Mater.,* 2010, **22**, 587.
8 C. Umrigar, D.E. Ellis, D.-S. Wang, H. Krakauer and M. Posternak, *Phys. Rev. B*, 1982, **26**, 4935.
9 Y.-S. Kim, H.-J. Kim, Y.-A. Jeon and Y.-M. Kang, *J. Phys. Chem. A,* 2009, **113**, 1129.
10 T. Kaewmaraya, M. Ramzan, J.M. Osorio-Guillen and R. Ahuja, *Solid State Ionics*, 2014, **261**, 17.
11 W. Kohn and L.J. Sham, *Phys. Rev., 1965,* **140**, A1133.
12 P. Giannozzi, et al., *J. Phys. Condens. Matter*., 2009, **21**, 395502.
13 A.D. Corso, *Comput. Mat. Sci*., 2014, **95**, 337.
14 J.P. Perdew, K. Burke and M. Ernzerhof, *Phys. Rev. Lett*., 1996, **77**, 3865.
15 H.J. Monkhorst and J.D. Pack, *Phys. Rev. B*, 1976, **13**, 5188.
16 M. Cococcioni and S. de Gironcoli, *Phys. Rev. B*, 2005, **71**, 35105.
17 H.J. Kulik, M. Cococcioni, D.A. Scherlis and N. Marzari, *Phys. Rev. Lett.*, 2006, **97**, 103001.
18 E. Levi, E. Lancry, A. Mitelman, D. Aurbach, G. Ceder, D. Morgan and O. Isnard, *Chem. Mater.*, 2006, **18**, 5492.
19 N.F. Mott, *Rev. Mod. Phys*., 1968, **40**, 677.
20 E. Levi and D. Aurbach, *Chem. Mater*., 2011, **23**, 1901.
21 M. D. Levi, E. Lancry, H. Gizbar, Y. Gofer, E. Levi and D. Aurbach, Electrochim. Acta 2004, **49**, 3201.
22 A. Simon, *Angew. Chem. Int. Ed. Engl*., 1988, **27**, 159.

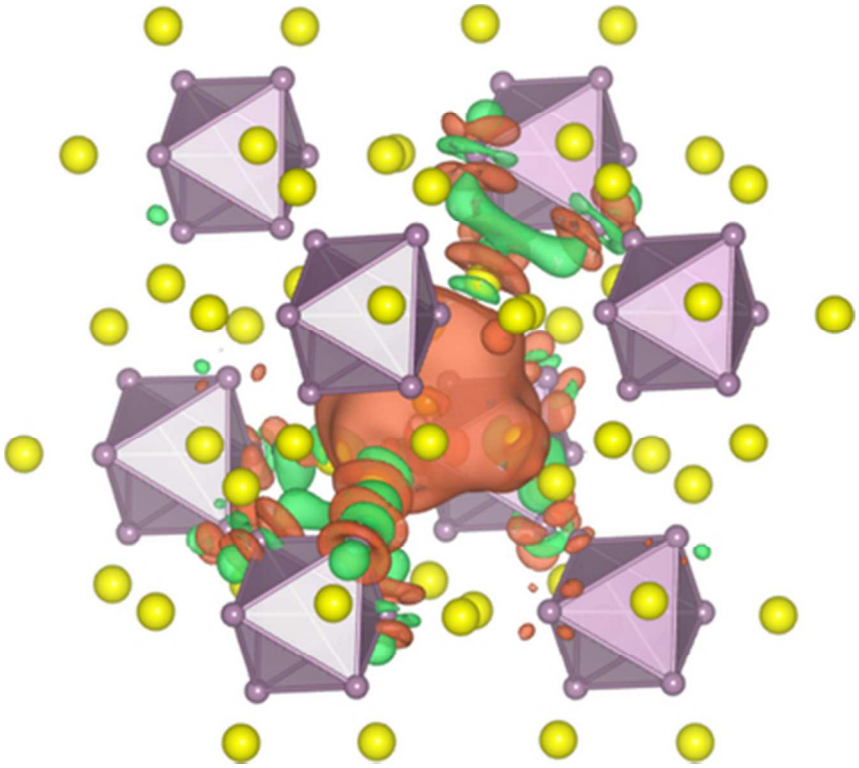

35x32mm (300 x 300 DPI)

The metallic Mo_6S_8 allows for highly localized electronic screening that shields the Mg 2+ charge and ease its diffusion.